Journal of Materials Chemistry A

ROYAL SOCIETY OF CHEMISTRY

PAPER

View Article Online
View Journal | View Issue

Cite this: J. Mater. Chem. A, 2025, 13, 2875

Accurately tuning the pore size and acidity of mesoporous zeolites for enhancing the catalytic hydrocracking of polypropylene†

Ziru Wang,[ab] Li Gao,[bc] Xia Zhong,[bc] Ying Zhang,[bd] Mozaffar Shakeri,[e] Xia Zhang *[a] and Bingsen Zhang *[bc]

Catalytic hydrocracking of plastics is one of the appealing strategies for converting waste plastics into high-value chemicals and fuels, featuring environmental friendliness and economy. Zeolites are considered to be promising catalysts for plastic hydrocracking. But there is still a distance from practical applications due to obstacles, such as the unsatisfactory catalytic efficiency and unclear influences of the active sites of zeolites on the catalytic performance. Herein, we synthesized a series of Al-MCM-41 catalysts with regulable specific surface area, pore size, and acidity by a sol–gel method, which were used for catalytic hydrocracking of polypropylene (PP) to clarify the structure–performance relationship. The results showed that the specific surface area and pore size of the zeolite were positively correlated with the catalytic performance of PP hydrocracking. Additionally, it was found that the acidity of the zeolite exhibited a peak distribution. Al-MCM-41 has a high liquid fuel yield (70.23%) at a lower hydrocracking temperature (220 °C) and is an efficient catalyst for PP hydrocracking. Furthermore, it was observed that zeolites with larger pore size and specific surface area can prolong the life of zeolites. The research can give a better understanding of how to design higher-performance and long-life catalysts for chemical upcycling of waste plastics.

Received 14th October 2024
Accepted 6th December 2024

DOI: 10.1039/d4ta07329k

rsc.li/materials-a

Introduction

The rapid growth of plastic waste has brought about serious environmental pollution problems. The traditional disposal process has shown huge environmental issues, such as the incineration of plastic waste producing large amounts of carbon dioxide and landfills containing hard-to-biodegrade plastics encroaching on large areas of land, that push the research toward more efficient processing.[1–4] Plastic waste can be transformed into micro- or nanoplastic particles, which may enter our drinking water or food systems and jeopardize human health.[5–7] Recycling plastic waste not only solves the abovementioned environmental pollution problem but also promotes economic benefits and contributes to achieving carbon neutrality.[8–11] To date, a huge amount of plastic waste is generated every year, but only a small portion of the plastic is recycled, and the treatment and recycling of plastic waste has attracted global attention.[12,13] Catalytic hydrocracking of plastics can convert waste plastics into higher value-added chemicals and fuels, which is an environmentally friendly and economical method of recycling plastic waste.[14,15] At present, plastic hydrocracking focuses on the development of efficient catalysts to improve the product yield and selectivity, as well as optimize pyrolysis parameters and reduce reaction costs.[16,17]

Polyolefins, such as high-density polyethylene (HDPE), low-density polyethylene (LDPE), and polypropylene (PP), are the most abundant of the waste plastics, accounting for more than half of the total plastic demand.[18,19] Among them, polypropylene has high spatial site resistance, and its diffusion is easily limited, making catalytic hydrocracking more difficult.[20–22] MCM-41, a mesoporous zeolite with relatively large pore volume, high specific surface area, and shape selectivity for value-added hydrocarbons, is commonly used in the catalytic hydrocracking of polypropylene.[23–25] However, MCM-41 itself is weakly acidic, which is not conducive to the catalytic hydrocracking reaction. After adding Al to the structure of MCM-41, the Si^{4+} atoms of MCM-41 are replaced by Al^{3+} atoms,

[a]Department of Chemistry, College of Science, Northeastern University, Shenyang 110819, China. E-mail: xzhang@mail.neu.edu.cn

[b]Shenyang National Laboratory for Materials Science, Institute of Metal Research, Chinese Academy of Sciences, Shenyang 110016, Liaoning, China. E-mail: bszhang@imr.ac.cn

[c]School of Materials Science and Engineering, University of Science and Technology of China, Shenyang 110016, Liaoning, China

[d]School of Petrochemical Engineering, Liaoning Petrochemical University, Fushun 113001, China

[e]Laboratory of Heterogeneous Catalysis Department of Chemical and Petroleum Engineering, Chemistry and Chemical Engineering Research Center of Iran, Tehran 16363, Iran

† Electronic supplementary information (ESI) available. See DOI: https://doi.org/10.1039/d4ta07329k

resulting in Brønsted and Lewis acid sites, which effectively enhance the acidity of MCM-41.[26,27]

After the process of plastic cracking, active intermediates are generated. These intermediates then enter the zeolites through their pores, where they are adsorbed to the acid sites of the zeolites and protonated. This results in the production of carbocation ions, which further lead to the generation of short-chain hydrocarbons. Therefore, the pore size and acidity of the zeolites play crucial roles in determining their catalytic performance.[28–30] The specific effects of the acidity and pore size of zeolites on the catalytic pyrolysis of plastics have been studied in a number of related areas. For example, Pyra *et al.*[31] used a series of FAU zeolites and mesoporous HAlMCM-48 catalysts with different silica–aluminum ratios and mesoporosities to study the effect of the presence of mesopores on the hydrocracking of polypropylene. Dai *et al.*[32] obtained ZSM-5 zeolites with a range of BAS concentrations and microporosities by post-processing ZSM-5 and investigated the effect of BAS and pore size on the service life of ZSM-5 zeolites in plastic hydrocracking. Most existing studies focus on adjusting the acidity and pore size of zeolites through post-treatment methods, such as desilication, dealuminization and dissolution recrystallization, which are time-consuming and costly. Furthermore, the correlation between the structure and properties in the catalytic cracking process of waste plastics has not been clearly elucidated. Therefore, it is expected to develop a simpler and faster method to study the structure–performance relationship of zeolites. Besides, how to prolong the life of the catalyst and adjust the product distribution efficiently and accurately to obtain high-value products is one of the important goals of developing new plastic cracking catalysts.

Herein, a series of Al-MCM-41 catalysts with varying specific surface areas and acidity were designed and synthesized by a sol–gel method for hydrocracking polypropylene, and then the effects of acidity and pore size on the cracking of PP by zeolites were investigated. In addition, the effect of mesopores on the catalyst life was also studied. The relationship between the physical and chemical properties of the catalyst and the reaction performance was determined by various characterization techniques. The experimental results indicated that there was a positive correlation between the specific surface area and pore size of the catalyst with the liquid fuel yield. Moreover, it was observed that acidity levels exhibited a peak distribution in relation to the liquid yield. Additionally, it was found that larger pore sizes could effectively prolong the life of zeolites.

Results and discussion

Catalyst characterization

Powder X-ray diffraction (XRD) was used to characterize the microstructure of the synthesized products. As can be seen from Fig. 1, all the samples have similar diffraction peaks, indicating that changing the raw material ratios did not change the crystal phase of the zeolites, and the peaks appearing around 2° correspond to the (100) diffraction peaks of MCM-41 (JCPDS 49-1712). The introduction of aluminum into MCM-41 leads to a change in the Al–O–Si bond angle, resulting in a wider (100) diffraction peak and a shift of the XRD peak towards a higher 2θ value. Moreover, the diffraction peaks (110) and (200) disappear in all samples except for L3.[33,34]

The TEM images with particle size distribution (PSD) frequency histograms of H1, H2, and H3 are shown in Fig. 2, and all zeolites showed regular porous nanosphere structures. By adjusting the NaOH/Si content in raw materials, the average diameter of nanospheres changed. The average diameter of H1, H2, and H3 samples was 43.98 nm, 55.67 nm, and 81.98 nm, respectively, indicating that the diameter of nanospheres gradually elevated with the increase of alkali content. This is due to the formation of large micelles during the sol formation process. According to the HAADF-STEM images and EDX elemental maps of H1, H2, and H3 shown in Fig. S2,† the expected elements including O, Si, and Al are evenly distributed.

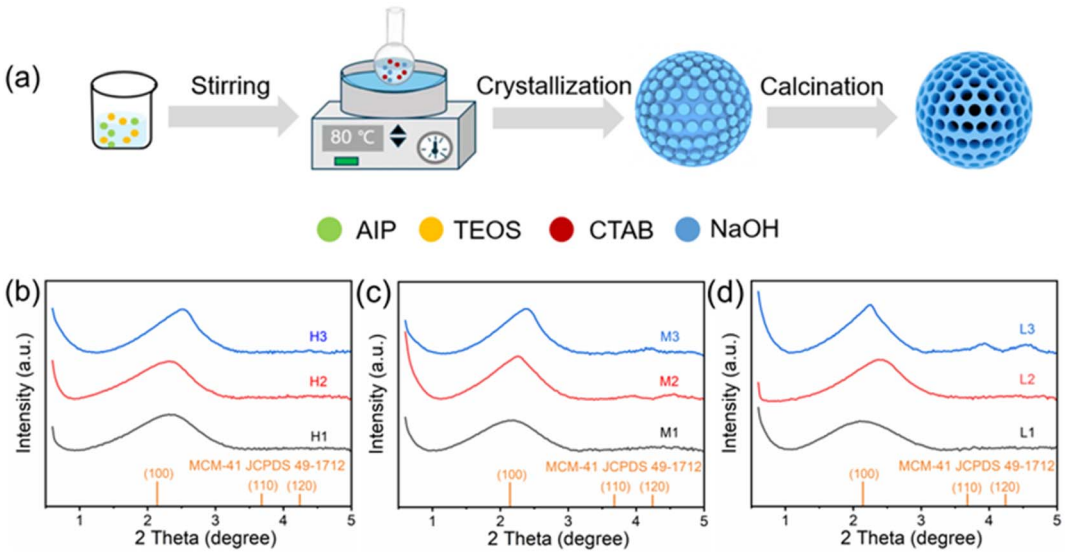

Fig. 1 Schematic diagram of the preparation of Al-MCM-41 catalysts (a). XRD patterns of different Al-MCM-41 catalysts (b–d).

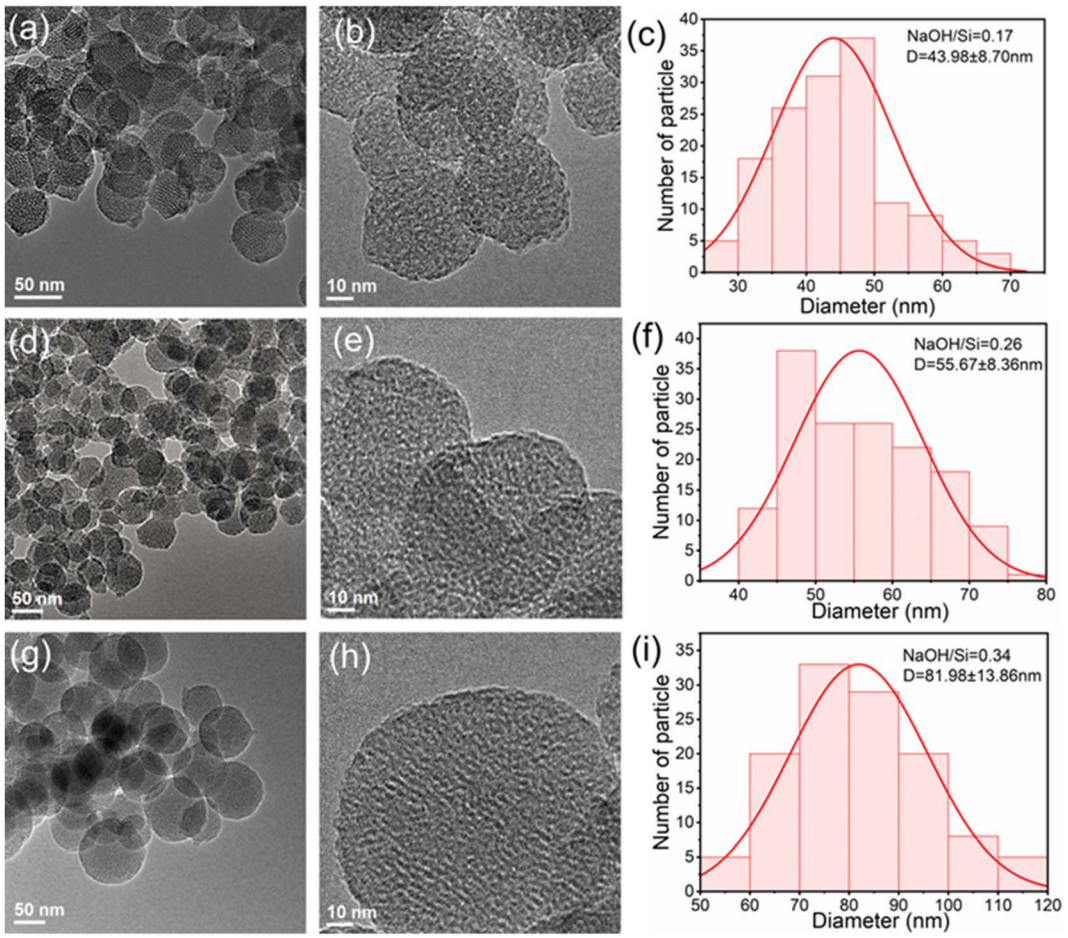

Fig. 2 TEM images and particle size distribution (PSD) frequency histograms of H1 (a–c), H2 (d–f), and H3 (g–i).

After adjusting the Al content in the catalyst, TEM images, HAADF-STEM images, and EDX element maps were recorded, which are presented in Fig. S3–S8.† The zeolite still exhibits a porous nanosphere structure with a uniform distribution of various elements. However, with the decrease of Al content, the edges of the nanospheres gradually dissolve and connect with each other, resulting in an increase in irregularity, especially for H3, M3 and L3 samples, and the same observation has been

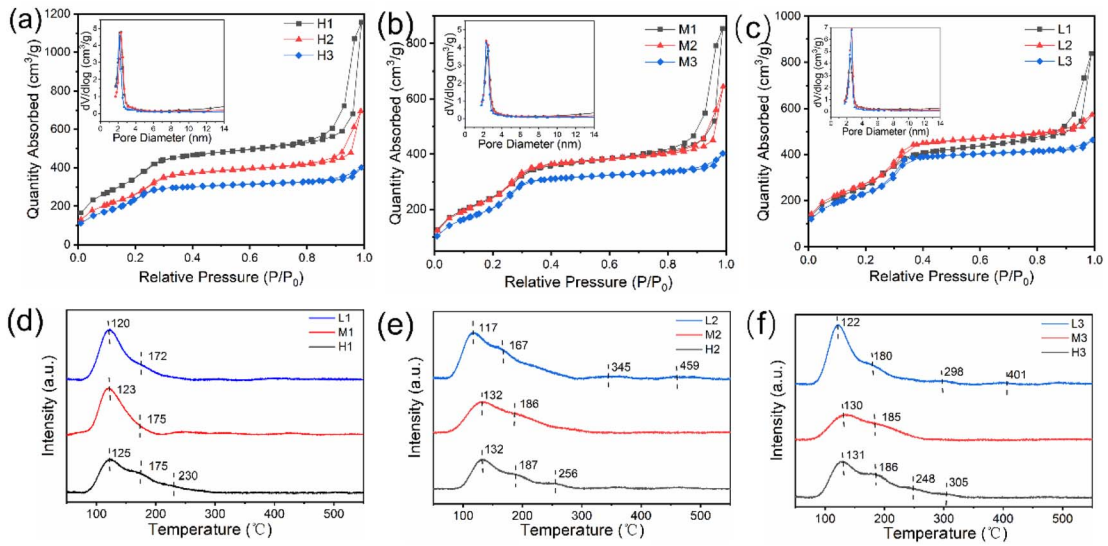

Fig. 3 N_2 adsorption–desorption isotherms with pore size distribution curves (a–c) and NH_3-TPD curves (d–f) of different Al-MCM-41 catalysts.

Table 1 Chemical composition and textural properties of the Al-MCM-41 catalysts

Samples	S_{BET} (m^2 g^{-1})	$S_{external}$ (m^2 g^{-1})	Pore volume (cm^3 g^{-1})	Average pore size (nm)	Si/Al	NaOH/Si
H1	1448.46	2031.84	1.898	4.941	5	0.17
H2	1112.01	1455.25	1.158	3.862	5	0.26
H3	991.57	1463.63	0.662	2.053	5	0.34
M1	1009.52	1215.68	1.372	5.231	15	0.17
M2	1025.06	1443.33	1.050	3.888	15	0.26
M3	894.10	1312.16	0.669	2.783	15	0.34
L1	1104.49	1390.04	1.245	4.690	30	0.17
L2	1089.15	1376.78	0.946	3.253	30	0.26
L3	923.85	1390.05	0.768	3.103	30	0.34
M1 used	735.84	907.15	1.312	6.931	15	0.17
M2 used	680.93	820.30	0.744	4.064	15	0.26
M3 used	623.37	740.05	0.714	4.606	15	0.34

reported already in the published literature.[35] The SEM images of the samples are shown in Fig. S9,† and all the samples are stratospheric, which is consistent with the TEM images.

Detailed information about the pore structure was obtained from N_2 adsorption–desorption isotherm curves and BJH pore size distributions. As shown in Fig. 3a–c, the N_2 adsorption–desorption isotherms of all catalysts are type IV, which confirms that the synthesized catalysts have a typical mesoporous structure.[36] Hysteresis loops appear at a P/P_0 value of 0.9–1.0, indicating that capillary condensation occurs here and large mesopores exist.[37] Obvious differences in the size of hysteresis loops of samples indicate different pore sizes. It can be seen from Fig. S10† and Table 1 that all catalysts show a high specific surface area, the specific surface area changes in a gradient manner, and the pore size is basically positive with the specific surface area. According to BET results, the pore size and specific surface area can be effectively adjusted by changing the ratio of raw materials during synthesis.

NH_3-TPD was used to investigate the surface acidity of zeolites, and the acidity intensity is positively correlated with the NH_3 desorption temperature. The NH_3-TPD curves of Al-MCM-41 show two broad peaks corresponding to weak acid sites at 100–200 °C (Fig. 3d–f), indicating that Al-MCM-41 possesses a large amount of acidity, but there are no strong acid sites. With the increase of Al content, the peak position is gradually shifted to a high temperature, indicating that the acidity of Al-MCM-41 becomes stronger gradually. For Al-MCM-41 with a Si/Al ratio of 5, the NH_3 desorption peak appears at 230–305 °C, suggesting the presence of medium-strong acid sites. Samples L2 and L3 exhibit weak NH_3 desorption peaks at 250–350 °C and 400–500 °C, indicating the presence of medium-strong acid sites and strong acid sites, albeit with a lower acid content. This can be attributed to the incorporation of NaOH and Al^{3+} into MCM-41, which enhances the surface acidity.[38] Combining the results of NH_3-TPD and BET, it is concluded that the acid density and pore size can be effectively adjusted by modifying the ratio of raw materials during synthesis.

Catalytic performances for PP hydrocracking

In this section, PP was subjected to hydrocracking at 220 °C under 2 MPa H_2 for 12 h in order to assess the impact of acidity and pore size on PP catalytic cracking. The reaction scheme and results are shown in Fig. 4a–e. Among the catalysts employed in PP hydrocracking, the highest conversion rate of PP was observed in sample M2, reaching 83.69%, with a corresponding liquid yield of 64.93% (Fig. 4b). Conversely, sample M1 exhibited a slight decline in the conversion rate (80.62%), yet achieved the highest liquid yield (70.23%), indicating that suitable acidity and specific surface area are crucial to the catalytic hydrocracking of PP by zeolites. With the decrease of specific surface area, the conversion rate of PP in zeolite catalytic hydrocracking exhibited a declining trend, while the liquid yield decreased more obviously. The effect of pore size was analyzed from the reaction mechanism. Following the cracking of PP on the outer surface of the zeolite, the intermediates diffused into the mesopores. The active site for catalytic reactions is located at the protic acid center of tetrad coordination aluminum within the wall of Al-MCM-41, where further cracking of intermediates occurs. The pore size plays a crucial role in affecting both the adsorption and diffusion of intermediates and products. Larger pores can enhance zeolite diffusion, reduce product molecule residence time, and minimize the probability of side reactions.[39]

The specific surface area and pore size of samples H2, M2, and L2 showed minimal changes, but a significant difference in liquid yield was observed, indicating that a moderate degree of acidity plays a vital role in promoting the catalytic hydrocracking of PP. Excessive acidity may result in excessive hydrocracking of C–C bonds, which in turn leads to poor selectivity of liquid fuel and the production of more gaseous products.[40] As a result, the products of H1, H2, and H3 samples are mainly gaseous products. As illustrated in Fig. 4d and e, with the increase in pore size, the proportion of olefins in the gaseous product increases, indicating that high olefin production is related to the highly developed mesoporous outer surface of the catalyst. This is due to the shorter diffusion path, which reduces the likelihood of alkenes becoming saturated through hydride transfer reactions. Ultimately, this helps to improve the yield of light alkenes.[41] The proportion of C_{15}–C_{21} in the liquid product increases, meaning that more heavy hydrocarbons are generated. This is attributed to the shape selectivity of the zeolite,

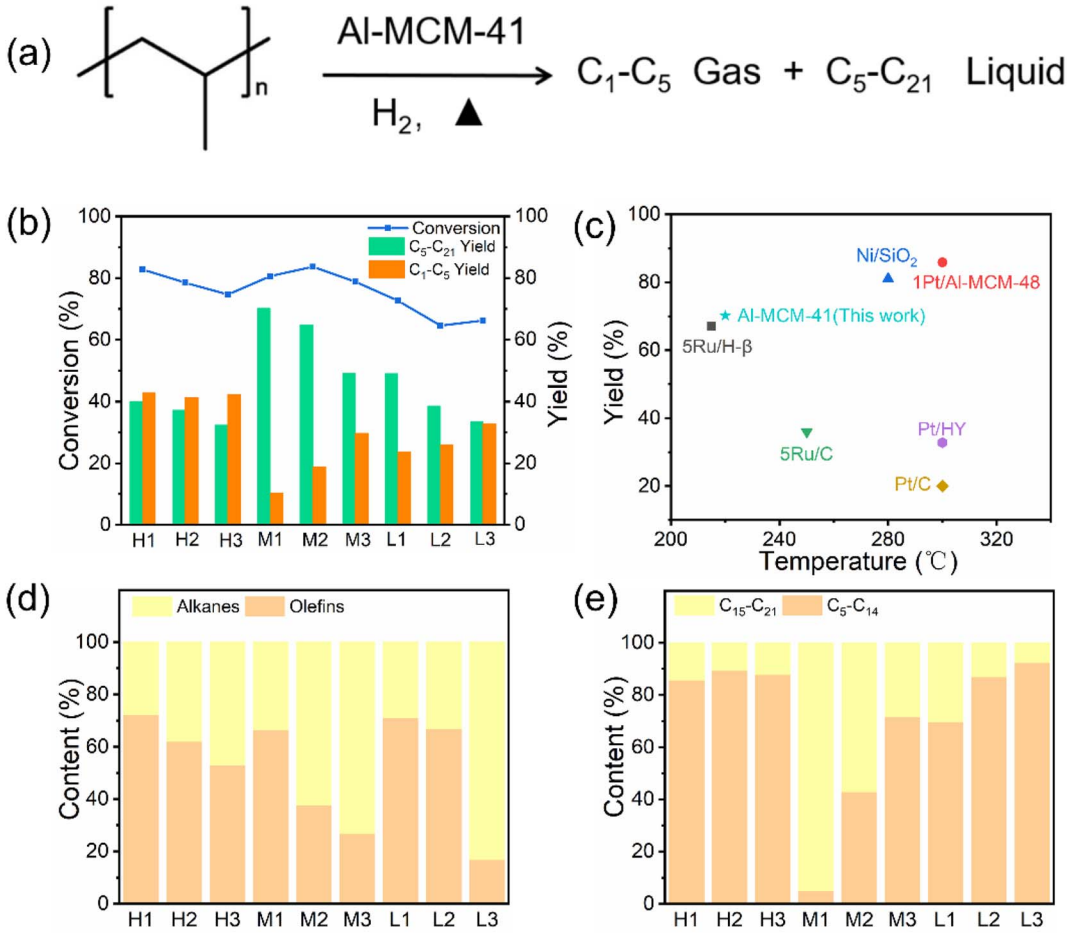

Fig. 4 The reaction scheme of the PP hydrocracking reaction (a). Conversion and product yield (b) of different Al-MCM-41 catalysts (reaction conditions: 220 °C, 2 MPa H_2, and 12 h). Performance comparison of polyolefin upcycling in this work with the reported catalysts (c). Olefin selectivity in gaseous products (d), and C_{15}–C_{21} selectivity in liquid products (e) of different Al-MCM-41 catalysts (reaction conditions: 220 °C, 2 MPa H_2, 12 h, 30 mg PP, and 30 mg catalyst).

where the reaction intermediate diffuses slowly through narrow pores, leading to secondary cleavage into smaller products. Above all, the pore size and acidity of Al-MCM-41 can effectively regulate the distribution of catalytic hydrocracking products. Given that sample M2 provided the highest PP conversion and excellent liquid yield among Al-MCM-41, it was selected for follow-up studies.

Catalytic hydrocracking reactions of PP were performed on Al-MCM-41 at elevated reaction temperatures and with different reaction times, to elucidate the potential mechanisms of C–C bond cleavage on zeolites and identify optimum reaction conditions. At the elevated reaction temperature (Fig. S11a†), the conversion rate of PP continuously increases, meanwhile the liquid yield also increases with the elevated temperature and reaches the highest at 220 °C, indicating that more gas is produced at temperatures higher than 220 °C. Then, the time-dependent experiments were conducted with catalysts at 220 °C (Fig. S11b†). The PP conversion increased continuously with extension of time from 4 h to 16 h. The highest liquid yield was achieved at a reaction time of 12 h, which means that the selectivity to the gas increases after 12 h. In summary, the optimal experimental conditions for the catalytic cracking reaction of PP over the Al-MCM-41 catalyst are 220 °C and 12 h, which feature a relatively low reaction temperature compared to other catalysts used for plastic cracking in the literature (Fig. 4c and Table S1†).

Effect of pore size on the life of zeolites

In this section, M1, M2, and M3 were selected as catalysts. After each reaction, the catalysts were washed and dried to prepare for the next operation. No new catalysts were introduced to compensate for any loss of catalysts during previous operations. In each reaction, the amount of PP injected was the same as the first time (30 mg). This was done to investigate the effects of different specific surface areas and pore sizes on the life of the zeolites. As illustrated in Fig. 5b–d, when three samples were introduced into PP for the second time, the conversion rate was slightly increased; meanwhile, the liquid yield decreased and more gas was produced. The conversion rate increased after the second injection, probably due to the secondary reaction of the previous residue. Furthermore, it is normal for conversion rates

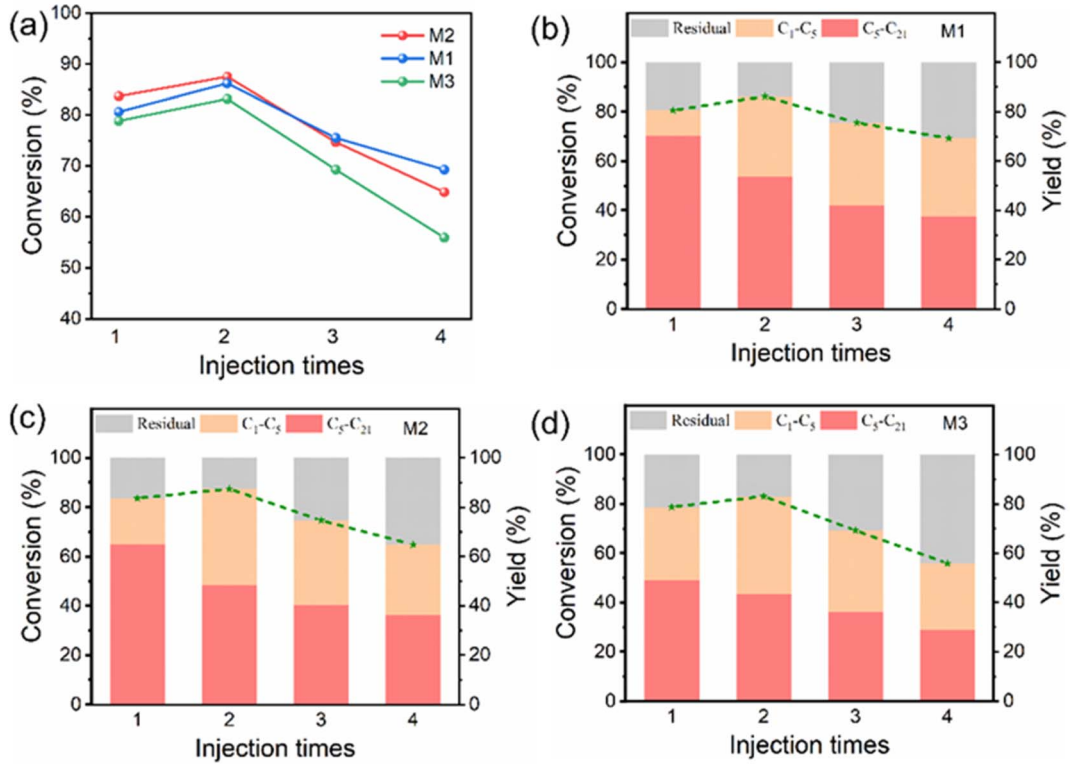

Fig. 5 Comparison of conversion rates of M1, M2, and M3 (a). Conversion and product yield of PP hydrocracking over M1 (b), M2 (c), and M3 (d) catalysts at different PP injection times. Reaction conditions: 220 °C, 2 MPa H_2, 12 h, 30 mg PP, and 30 mg catalyst.

to fluctuate in the cycle, and this phenomenon has also appeared in the published literature.[42,43] After the third injection of PP, both the conversion rate and liquid production rate decreased because the catalyst was gradually deactivated with the increase of reaction times. As shown in Fig. 5a, the decline rate of the conversion rate follows the order of M3 > M2 > M1. The conversion rate of M1 exhibited the smallest decrease, indicating that the M1 catalyst demonstrated greater stability, which may be because the larger specific surface area and pore size can provide a shorter diffusion channel and more space for coke deposition, slow the coke accumulation rate, and then affect the deactivation rate of the zeolite. In order to further verify this, the amount of coke present in the used catalyst was assessed through thermogravimetric analysis (Fig. S12†). The first phase of weightlessness is due to water desorption and the second phase is due to organic residues (200–400 °C). The weight loss observed above 400 °C is primarily attributed to the presence of coke.[44,45] The coke content for sample M1 is measured to be 2.6%, while that for M2 is 4.6%, and for M3 it reaches 8.7%. Obviously, the catalyst sample M1 demonstrated excellent catalytic stability. With the increase of the amount of PP, the selectivity of catalytic hydrocracking products to gas increases, and the selectivity of high-value liquid products decreases. The TEM images, XRD patterns, NH_3-TPD curves, and N_2 adsorption–desorption isotherms of the used catalysts are shown in Fig. S13, S14† and Table 1, and the morphology and structure of the catalysts did not change significantly. The N_2 adsorption–desorption isotherms of the catalysts are all still type IV, and the specific surface area, pore size and pore volume of the catalysts are seen to decrease slightly. However, the acidity of the catalyst decreased significantly. The decrease of the specific surface area, pore size, pore volume and acidity of the used catalysts resulted in the decrease of conversion rate. In summary, the experiment proves that the pore size of zeolites is very important to the life of zeolites, and the larger pore size and specific surface area can prolong the life of zeolites.

Conclusions

In summary, a series of Al-MCM-41 catalysts with changeable specific surface area, pore size, and acidity were synthesized by a sol–gel method for catalytic hydrocracking of PP to reveal the structure–performance relationship of zeolites. Our results show that Al-MCM-41 is an efficient catalyst with a high liquid fuel yield (70.23%) at a lower hydrocracking temperature (220 °C). The specific surface area and pore size of the zeolite were positively correlated with the catalytic performance of PP hydrocracking. Meanwhile, it was found that the acidity of the zeolite exhibited a peak distribution. Besides, larger pore size and specific surface area can prolong the life of the zeolite. The research has guiding significance for the design of catalysts with high-value liquid fuel yield and long life. In addition, this study highlights the importance of designing zeolites with appropriate acidity and pore size to improve the performance of zeolites in plastic hydrocracking.

Experimental section

Chemicals

Absolute ethanol (99.9%, AR), tetraethyl orthosilicate (TEOS, 99.9%, AR), aluminum isopropoxide ($Al(OiPr)_3$), hexadecyltrimethylammonium bromide (CTAB), and mesitylene (99.9%, AR) were purchased from Beijing InnoChem Science & Technology Co., Ltd. Sodium hydroxide (NaOH) and trichloromethane ($CHCl_3$, ≥99.0%) were purchased from Sinopharm Chemical Reagent Co., Ltd. Deionized water was prepared in a laboratory.

Synthesis of samples

118.8 mg of aluminum isopropyl alcohol was dissolved in 32 mL ethanol, then the solution was stirred for 1 hour. 1.944 mL of tetraethyl orthosilicate was added to the solution and stirred for 30 minutes to prepare solution (A). Solution (B) was prepared by mixing 153.6 mL of distilled water with 1.12 mL of 2 M sodium hydroxide solution and 0.32 g of cetyltrimethylammonium bromide and stirring at 300 rpm in a reflux system at 80 °C. Solution (A) was added to solution (B) in drops, and the resulting mixture was stirred at 80 °C at 300 rpm for 2 hours. After the solution was cooled to room temperature, the solid was collected by centrifugation and rinsed with distilled water until neutral, and then dried at 80 °C. The dried samples were heated from room temperature at a rate of 3 °C min^{-1} to 600 °C and treated at constant temperature for 5 hours. By adjusting the raw material ratio (Si/Al = (5, 15, 30) and NaOH/Si = (0.17, 0.26, 0.34)) for the synthesis of Al-MCM-41, nine samples with different specific surface areas and acidity were synthesized. According to the sample acidity, from strong to weak, it was denoted as H, M and L. According to the pore size and specific surface area of the sample, it was denoted as 1, 2 and 3 from the largest to the smallest, as shown in Table 1.

Characterization

X-ray diffraction (XRD) was used to characterize the crystal structure of the catalysts on a SmartLab diffractometer, which collected data using a Cu Kα source (λ = 1.5406 Å) in the 2θ range from 1 to 5°. Transmission electron microscopy (TEM) images, high-angle annular dark-field-scanning TEM (HAADF-STEM) images, and EDX elemental maps were acquired using an FEI Tecnai G2 F20 transmission electron microscope equipped with HAADF and EDX detectors. The Brunauer–Emmett–Teller (BET) specific surface area and Barrett–Joyner–Halenda (BJH) pore distribution were measured by N_2 adsorption–desorption on a Micromeritics ASAP 2020, and all catalysts were degassed for 4 h before the measurement. Temperature-programmed desorption of NH_3 (NH_3-TPD) patterns were recorded using a mass spectrometer (Pfeiffer OmniStar). The weighed sample (30 mg) was loaded into the quartz tube reactor and then heated to 550 °C for 30 min with a He flow rate of 30 mL min^{-1}. After that, the temperature was cooled down to 50 °C. NH_3–He (10 vol% NH_3) at a flow rate of 30 mL min^{-1} was introduced into the reactor for 40 min. The sample was then purged with He for 40 min. And the temperature was ramped from 50 °C to 600 °C at 10 °C min^{-1}. The thermogravimetric analysis measurements were performed on a HITACHI STA200 simultaneous thermal analyzer with a heating rate of 10 °C min^{-1} from room temperature to 800 °C in an air atmosphere.

Catalytic performance test of the PP hydrocracking reaction

The PP hydrocracking reaction was carried out in a 50 mL stainless steel autoclave with stirring. Fig. S1† shows the schematic of the reactor. Typically, the catalyst and PP were mixed evenly and loaded into the autoclave with the ratio of PP to catalyst kept at 1 : 1. Before the reaction, argon gas was used to remove the air from the autoclave and check the air tightness. Then, 2 MPa hydrogen was injected into the autoclave and heated to 220 °C. When it was heated to 160 °C, stirring at 600 rpm was initiated. After the reaction, the autoclave was cooled down to room temperature. The gaseous products were collected using a gas bag. To obtain the liquid product, 10 mL of $CHCl_3$ and 30 μL of mesitylene were used as the solvent and internal standard to recover the solution from the autoclave. After the mixture became uniform, a certain amount of solution was taken out and filtered into a chromatographic bottle through the organic filter head. The solid residue was separated from the remaining mixture, which was then washed, dried, and weighed. The gaseous (C_1 to C_5) and liquid (C_5 to C_{21}) products were analyzed using a gas chromatograph (GC) equipped with a flame ionization detector (FID). The PP conversion and product yields were calculated using the following equations:

$$\text{PP conversion}(\%) = \left[1 - \frac{m(\text{residuals}) - m(\text{catalyst})}{m(\text{PP})}\right] \times 100\%$$

$$\text{Product yield}(\%) = \frac{m(C_x)}{m(\text{PP})} \times 100\%$$

$$\text{Olefins selectivity in gaseous products}(\%) = \frac{m(\text{Olefins})}{m(C_1 - C_5)} \times 100\%$$

$$C_{15} - C_{21} \text{ selectivity in liquid products}(\%) = \frac{m(C_{15} - C_{21})}{m(\text{liquid})} \times 100\%$$

Data availability

Data will be made available on request.

Author contributions

The manuscript was written through contributions of all authors. All authors have given approval to the final version of the manuscript.

Conflicts of interest

There are no conflicts to declare.

Acknowledgements

The authors gratefully acknowledge the financial support provided by the National Natural Science Foundation of China (No. 52161145403), the Research Fund of Shenyang National Laboratory for Materials Science and the Iran National Science Foundation (4001399).

References

1 X. Si, J. Chen, Z. Wang, Y. Hu, Z. Ren, R. Lu, L. Liu, J. Zhang, L. Pan, R. Cai and F. Lu, *J. Energy Chem.*, 2023, **85**, 562–569.
2 Q. Cao, X.-F. Cheng, J. Wang, C. Zhou, L.-J. Yang, G. Wang, D.-Y. Chen, J.-H. He and J.-M. Lu, *Chin. Chem. Lett.*, 2024, **35**, 108759.
3 R. J. Conk, S. Hanna, J. X. Shi, J. Yang, N. R. Ciccia, L. Qi, B. J. Bloomer, S. Heuvel, T. Wills, J. Su, A. T. Bell and J. F. Hartwig, *Science*, 2022, **377**, 1561–1566.
4 A. Rahimi and J. M. Garcia, *Nat. Rev. Chem.*, 2017, **1**, 0046.
5 M. Z. Shah, M. Quraishi, A. Sreejith, S. Pandit, A. Roy and M. U. Khandaker, *Chemosphere*, 2024, **352**, 141451.
6 S. Y. Choi, Y. Lee, H. E. Yu, I. J. Cho, M. Kang and S. Y. Lee, *Nat. Microbiol.*, 2023, **8**, 2253–2276.
7 J. Deng, L. Meng, D. Ma, Y. Zhou, X. Wang, X. Luo and S. Yuan, *J. Energy Chem.*, 2023, **80**, 215–227.
8 S. D. A. Sharuddin, F. Abnisa, W. M. A. W. Daud and M. K. Aroua, *Energy Convers. Manage.*, 2017, **148**, 925–934.
9 J. R. Jambeck, R. Geyer, C. Wilcox, T. R. Siegler, M. Perryman, A. Andrady, R. Narayan and K. L. Law, *Science*, 2015, **347**, 768–771.
10 L. Li, H. Luo, Z. Shao, H. Zhou, J. Lu, J. Chen, C. Huang, S. Zhang, X. Liu, L. Xia, J. Li, H. Wang and Y. Sun, *J. Am. Chem. Soc.*, 2023, **145**, 1847–1854.
11 M. S. Abbas-Abadi, Y. Ureel, A. Eschenbacher, F. H. Vermeire, R. J. Varghese, J. Oenema, G. D. Stefanidis and K. M. Van Geem, *Prog. Energy Combust. Sci.*, 2023, **96**, 101046.
12 R. Geyer, J. R. Jambeck and K. L. Law, *Sci. Adv.*, 2017, **3**, e1700782.
13 M.-Q. Zhang, M. Wang, B. Sun, C. Hu, D. Xiao and D. Ma, *Chem*, 2022, **8**, 2912–2923.
14 A. J. Martin, C. Mondelli, S. D. Jaydev and J. Perez-Ramirez, *Chem*, 2021, **7**, 1487–1533.
15 J. Du, L. Zeng, T. Yan, C. Wang, M. Wang, L. Luo, W. Wu, Z. Peng, H. Li and J. Zeng, *Nat. Nanotechnol.*, 2023, **18**, 772–779.
16 X. Chen, Y. Wang and L. Zhang, *ChemSusChem*, 2021, **14**, 4137–4151.
17 J. M. Garcia and M. L. Robertson, *Science*, 2017, **358**, 870–872.
18 R. Mishra, A. Kumar, E. Singh and S. Kumar, *ACS Sustain. Chem. Eng.*, 2023, **11**, 2033–2049.
19 J. Huang, A. Veksha, W. P. Chan, A. Giannis and G. Lisak, *Renewable Sustainable Energy Rev.*, 2022, **154**, 111866.
20 Y. Peng, Y. Wang, L. Ke, L. Dai, Q. Wu, K. Cobb, Y. Zeng, R. Zou, Y. Liu and R. Ruan, *Energy Convers. Manage.*, 2022, **254**, 115243.
21 N. K. Ciliz, E. Ekinci and C. E. Snape, *Waste Manag.*, 2004, **24**, 173–181.
22 R. Miandad, M. A. Barakat, A. S. Aburiazaiza, M. Rehan, I. M. I. Ismail and A. S. Nizami, *Int. Biodeterior. Biodegrad.*, 2017, **119**, 239–252.
23 T. Sun, T. Lei, Z. Li, Z. Zhang, S. Yang, X. Xin, M. Zhang, X. He, Q. Zhang and L. Zhang, *Ind. Crops Prod.*, 2021, **171**, 113843.
24 X. Tian, Z. Zeng, Z. Liu, L. Dai, J. Xu, X. Yang, L. Yue, Y. Liu, R. Ruan and Y. Wang, *J. Cleaner Prod.*, 2022, **358**, 131989.
25 J. M. Escola, J. Aguado, D. P. Serrano, A. Garcia, A. Peral, L. Briones, R. Calvo and E. Fernandez, *Appl. Catal., B*, 2011, **106**, 405–415.
26 C. Perego and R. Millini, *Chem. Soc. Rev.*, 2013, **42**, 3956–3976.
27 P. Son Tung, M. B. Nguyen, G. H. Le, N. Trinh Duy, C. D. Pham, L. Thanh Son and T. A. Vu, *Chemosphere*, 2021, **265**, 129062.
28 Q. Wen, Q. Zhang, Z. Liu, H. Wang, S. Hao, F. Zhang, L. Zhang, Q. Han and G. Zheng, *J. Energy Chem.*, 2024, **96**, 509–515.
29 Z. Dong, W. Chen, K. Xu, Y. Liu, J. Wu and F. Zhang, *ACS Catal.*, 2022, **12**, 14882–14901.
30 J. Z. Tan, C. W. Hullfish, Y. Zheng, B. E. Koel and M. L. Sarazen, *Appl. Catal., B*, 2023, **338**, 123028.
31 K. Pyra, K. A. Tarach and K. Gora-Marek, *Appl. Catal., B*, 2021, **297**, 120408.
32 L. Dai, N. Zhou, K. Cobb, P. Chen, Y. Wang, Y. Liu, R. Zou, H. Lei, B. A. Mohamed, Y. Cheng and R. Ruan, *Appl. Catal., B*, 2022, **318**, 121835.
33 K. Bachari, R. Chebout, R. M. Guerroudj and M. Lamouchi, *Res. Chem. Intermed.*, 2012, **38**, 367–381.
34 J. M. Campos, J. P. Lourenco, A. Fernandes and M. R. Ribeiro, *Catal. Commun.*, 2008, **10**, 71–73.
35 R. Locus, D. Verboekend, R. Zhong, K. Houthoofd, T. Jaumann, S. Oswald, L. Giebeler, G. Baron and B. F. Sels, *Chem. Mater.*, 2016, **28**, 7731–7743.
36 A. Tennakoon, X. Wu, M. Meirow, D. Howell, J. Willmon, J. Yu, J. V. Lamb, M. Delferro, E. Luijten, W. Huang and A. D. Sadow, *J. Am. Chem. Soc.*, 2023, **145**, 17936–17944.
37 G.-X. Duan, Q. Chen, R.-R. Shao, H.-H. Sun, T. Yuan and D.-H. Zhang, *Chin. Chem. Lett.*, 2024, 109751.
38 J. C. Bedoya, R. Valdez, L. Cota, M. A. Alvarez-Amparan and A. Olivas, *Catal. Today*, 2022, **388**, 55–62.
39 L. Ye, W. Yang, J. Fan, X. Pu, X. Han, X. Qin, M. Ma, Z. Huang, T. Wang, K. Zhu, Y. Xu and J. Liu, *Chem. Eng. J.*, 2024, **482**, 148705.
40 X. Wu, X. Wang, L. Zhang, X. Wang, S. Song and H. Zhang, *Angew. Chem., Int. Ed.*, 2024, **63**, e202317594.
41 V. Blay, B. Louis, R. Miravalles, T. Yokoi, K. A. Peccatiello, M. Clough and B. Yilmaz, *ACS Catal.*, 2017, **7**, 6542–6566.

42 Z. Zhang, J. Wang, X. Ge, S. Wang, A. Li, R. Li, J. Shen, X. Liang, T. Gan, X. Han, X. Zheng, X. Duan, D. Wang, J. Jiang and Y. Li, *J. Am. Chem. Soc.*, 2023, **145**, 22836–22844.
43 D. H. Zhang, T. Jin, J. B. Peng, J. J. Ma, J. L. Zhang, X. Tian and M. Y. Ding, *Fuel*, 2023, **334**, 126588.
44 B. C. Vance, Z. Yuliu, S. Najmi, E. Selvam, J. E. Granite, K. Yu, M. G. Ierapetritou and D. G. Vlachos, *Chem. Eng. J.*, 2024, **487**, 150468.
45 E. Selvam, P. A. Kots, B. Hernandez, A. Malhotra, W. Chen, J. M. Catala-Civera, J. Santamaria, M. Ierapetritou and D. G. Vlachos, *Chem. Eng. J.*, 2023, **454**, 140332.